



## Notch-tensile behavior of $\text{Al}_{0.1}\text{CrFeCoNi}$ high entropy alloy

Subhasis Sinha<sup>1</sup>, Mageshwari Komarasamy<sup>2</sup>, Tianhao Wang<sup>2</sup>, Ravi Sankar Haridas,  
Priyanka Agrawal, Shivakant Shukla, Saket Thapliyal, Michael Frank, Rajiv S. Mishra<sup>\*</sup>

*Center for Friction Stir Processing, Department of Materials Science and Engineering, Advanced Materials and Manufacturing Processes Institute, University of North Texas, Denton, TX, 76207, USA*



### ARTICLE INFO

**Keywords:**

High entropy alloy  
Notch  
Tensile deformation  
Digital image correlation  
Finite element analysis

### ABSTRACT

Notch-tensile behavior of an  $\text{Al}_{0.1}\text{CrFeCoNi}$  high entropy alloy ( $\text{Al}_{0.1}\text{-HEA}$ ) was studied using V-notch geometry and with local strain mapping using digital image correlation (DIC). A notch-strength ratio of 1.51 indicated notch strengthening. Further analysis of stress-strain response supplemented with microstructural analysis revealed that, while the presence of notch results in strengthening due to work hardening by twinning induced plasticity, the notch also contributes strongly to geometrical softening in the non-uniform ductility regime, and accounts for the onset of failure. The strain localization behavior of  $\text{Al}_{0.1}\text{-HEA}$  due to the presence of V-notch was compared with three conventional alloys: Inconel 625 nickel-based superalloy, 304 stainless steel and Ti-6Al-4V titanium alloy. The study revealed that the nature of notch widening with increasing strain was dependent on material characteristics. The extent of notch widening impacted the local strain field and stress distribution, thereby influencing the propensity for crack initiation and growth. The experimental results were verified by finite element analysis.

### 1. Introduction

Geometric discontinuity-induced variation in mechanical response is inevitable in the engineering of structural components used in practical applications [1]. Therefore, study of the notch effect of materials is integral to safe design [2]. A notch introduces higher stress concentration and varies the triaxial state of stress in a test specimen or design component [3]. Interestingly, depending on material characteristics and notch geometry, the presence of a notch could lead to strengthening or weakening [2,4].

Several researchers have investigated notch deformation behavior in various conventional materials such as superalloys, titanium alloys, composites and steels [5–9]. Using digital image correlation (DIC) to measure strain localization and damage, and to characterize crack growth behavior and ductile fracture initiation [10–12], these studies discussed the effect of different stress state depending on notch geometry and type of loading [10]. Roth and Mohr also discussed the effect of strain rate in notched specimens of high-strength steels [13], while other researchers studied creep and fatigue behavior in notched specimens [14,15]. Some previous researchers discussed impact testing of notched

specimens of high entropy alloys (HEA) to obtain fracture toughness [16–21]. However, the lack of studies on the notch-tensile behavior of HEAs provides the scope for further investigation.

Therefore, the present investigation deals with the notch-tensile behavior of  $\text{Al}_{0.1}\text{CrFeCoNi}$  HEA (henceforth referred to as  $\text{Al}_{0.1}\text{-HEA}$ ). Note that  $\text{Al}_{0.1}\text{CrFeCoNi}$  is a well investigated single-phase HEA (with face centered cubic (f.c.c.) crystal structure). The aim of this study is to establish a benchmark of the notch deformation behavior (with a V-notch geometry) of the  $\text{Al}_{0.1}\text{-HEA}$  with respect to conventional materials such as nickel-based superalloy or steel or titanium alloy. In the present study, the V-notched and un-notched tensile behavior of  $\text{Al}_{0.1}\text{-HEA}$  was compared. Strain localization near the notch was measured using DIC. Microstructural characterization of the failed notch-tensile specimens was performed to differentiate the deformation mechanisms in the vicinity of the notch from the deformation mechanisms in the gage region away from the notch.

Finally, the notch-tensile behavior of Inconel 625 (IN625), 304 stainless steel (304SS) and Ti-6Al-4V (Ti64) was evaluated to compare the notch effect in  $\text{Al}_{0.1}\text{-HEA}$  with these three conventional high-temperature alloys. The comparison is based on the fact that  $\text{Al}_{0.1}$

\* Corresponding author.

E-mail address: [Rajiv.Mishra@unt.edu](mailto:Rajiv.Mishra@unt.edu) (R.S. Mishra).

<sup>1</sup> Current address: Department of Metallurgical Engineering, Indian Institute of Technology (Banaras Hindu University), Varanasi, 221005 India.

<sup>2</sup> Current address: Pacific Northwest National Laboratory, MSIN: K2-03, 902 Battelle Blvd., Richland, WA 99352 USA.

HEA is a twinning induced plasticity (TWIP) HEA [22–24], and each of the three conventional alloys has different deformation characteristics. 304SS is a low-strength, high-ductility alloy that exhibits twinning [25]. Ti64 is a high-strength, low-ductility alloy but does not exhibit twinning [26]. IN625 has a strength-ductility combination in between 304SS and Ti64 [27]. The objective of the comparison is to determine whether the notch deformation behavior (strain localization and damage in the vicinity of the notch) of  $\text{Al}_{0.1}\text{-HEA}$  is similar to any of the three conventional alloys. Also, we anticipate determining how strongly the material aspect (since each particular alloy has specific strength-ductility characteristics) influences strain localization due to the notch.

## 2. Materials and methods

### 2.1. Experimental

The primary material studied in the present investigation is an  $\text{Al}_{0.1}\text{CrFeCoNi}$  HEA. The material was homogenized, cold-rolled and annealed at 700 °C (973 K) for 2 h to obtain a grain size of the order of 4–5  $\mu\text{m}$ . Other alloys used for comparison include Inconel 625 nickel-based superalloy, 304 stainless steel and Ti-6Al-4V titanium alloy (referred to as IN625, 304SS and Ti64, respectively). The prior treatments of the as-received plates of the latter three alloys were IN625 and Ti64 in the annealed condition and 304SS in the hot rolled condition. The initial microstructure and grain size for all the four alloys are presented later.

Room-temperature tensile tests with and without notch were performed at quasi-static strain rate ( $10^{-3} \text{ s}^{-1}$ ) using an Instron Universal Testing Machine (UTM). The notch-tensile test was supplemented with DIC, wherein multiple virtual extensometers were used for local strain mapping. The gage area of the notch-tensile specimen was covered with

black-and-white speckle patterns on one side for DIC imaging. Fig. 1 (a) shows the specimen geometry and dimensions of the notch-tensile specimen. A V-notch geometry with an included angle of 60° was used. The tensile specimens were machined out from the alloy plates using electrical discharge machining. Microstructural characterization of undeformed specimens and fractured notch-tensile specimens, by scanning electron microscopy in backscattered electron mode (SEM-BSE) and electron backscatter diffraction (EBSD), were performed in a FEI Nova Nano SEM 230 with attached Hikari Super EBSD detector operated at 20 kV. Transmission electron microscopy (TEM) specimen of the  $\text{Al}_{0.1}\text{-HEA}$  was obtained from the near-notch region of the notch-tensile specimen by focused ion beam (FIB) milling process using FEI Nova 200 Nanolab Dual Beam FIB/FESEM. TEM characterization was carried out using a FEI Tecnai G2 F20 S-Twin 200 keV field emission TEM.

### 2.2. Modeling

Finite element modeling of notch-tensile behavior was performed in a commercially available software ABAQUS to understand the stress distribution around the notch for all the four alloys. The modeling was performed with a 1/8 symmetric geometric model of the specimen by virtue of its symmetry along x, y and z axis as shown in Fig. 2 (a). A schematic of the meshed model is shown in Fig. 2(b). 3D C3D8R brick elements with reduced integration and hourglass control were used for the meshing. The symmetric boundary conditions in x, y and z directions were applied on faces shown in Fig. 2(b). A displacement boundary condition was applied on the face marked as A in Fig. 2(b). An extremely refined mesh, as shown in the inset of Fig. 2(b), was generated around the notch in order to avoid the mesh distortion due to substantial plastic deformation which would develop around the notch. All the alloys were

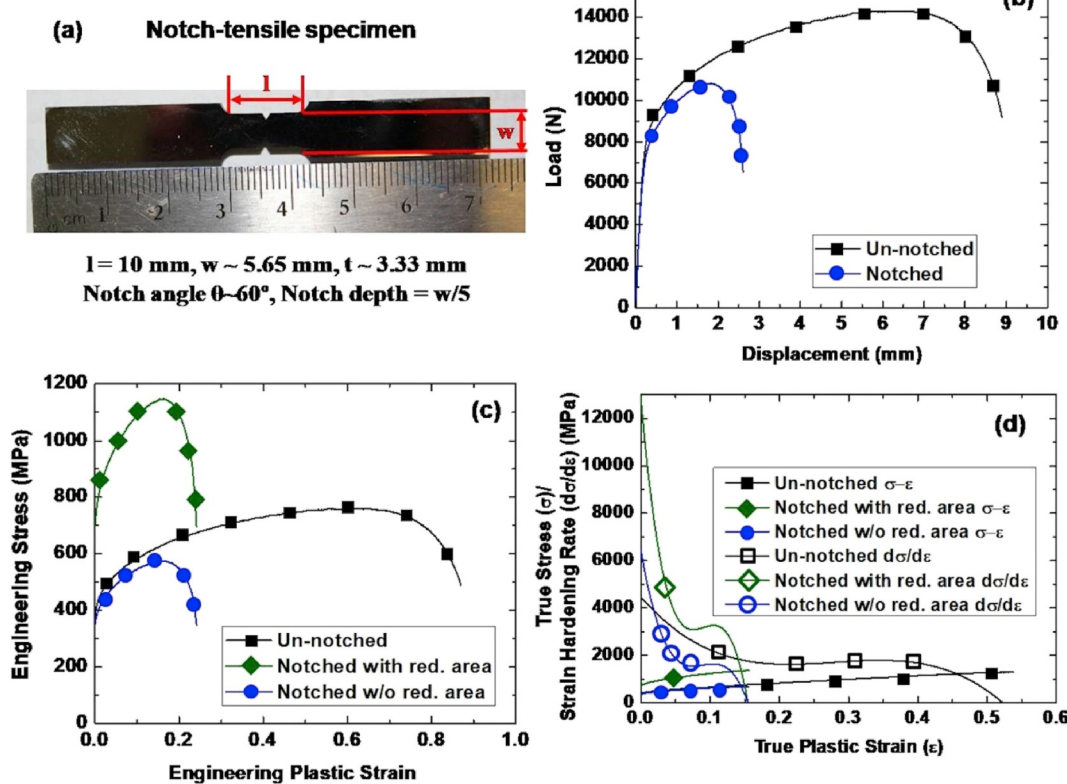


**Fig. 1.** (a) Notch specimen geometry and dimensions, (b) tensile load-displacement curves, (c) engineering stress-strain curves, and (d) true stress-strain and strain hardening rate curves for notched and un-notched specimens of  $\text{Al}_{0.1}\text{-HEA}$ . (Note: The symbols in (b–d) are included for easy reference to the graph legends and do not represent the number of data points plotted).

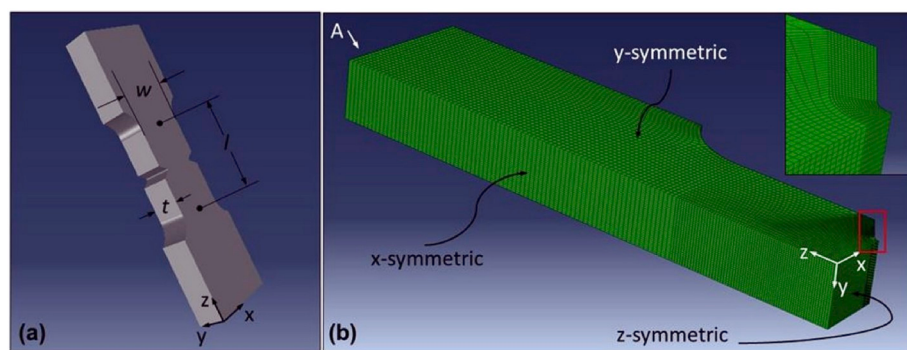


**Fig. 2.** (a) Geometry of the specimen indicating the symmetry along all three axes, and (b) schematic of the meshed model along with the symmetric boundary conditions.

assumed elastic-plastic with isotropic hardening and the post yield stress-plastic strain response of the materials obtained from the respective quasi-static tensile test was input in the model.

### 3. Results and discussion

#### 3.1. Notch-tensile response of $Al_{0.1}$ -HEA

**Fig. 1** (b) shows the tensile load-displacement curves of the notched and un-notched specimens of  $Al_{0.1}$ -HEA. The corresponding engineering stress-strain and true stress-strain curves are presented in **Fig. 1** (c) and (d), respectively. Notch-strength ratio (NSR) is used to quantify the strengthening or weakening effect of the notch, and is defined by equation (1) [2],

$$NSR = \text{Nominal UTS of notched specimen} / \text{Nominal UTS of un-notched specimen} \quad (1)$$

where UTS is the ultimate tensile strength.

The material is regarded as notch-strengthening when  $NSR > 1$ , while the material is regarded as notch-weakening when  $NSR < 1$ . While plotting the stress-strain curve and calculating NSR, we must consider the reduced cross-sectional area for the notched specimen. Otherwise, if the original cross-sectional area without reduction is considered for the notched specimen, the correct engineering stress cannot be obtained for the notched specimen. This is illustrated for the present  $Al_{0.1}$ -HEA specimens in **Fig. 1** (c) and (d) by considering both the notched specimen curves with and without reduced cross-sectional area. **Fig. 1** (c) and (d) depict clearly that, while ductility of the notched specimen is much lower compared to the un-notched specimen, the presence of notch leads to strengthening (comparison of black and green curves). The NSR value of 1.51 was obtained from the ratio of engineering UTS values in notched condition with reduced area and un-notched condition, thus quantifying the strengthening contribution from the notch.

Although the NSR is an established standard parameter to quantify the strengthening or weakening capability of a notch in a material and undoubtedly provides an appropriate estimate of the same, the limitation of this parameter is that it is based only on UTS values. The UTS value characterizes the peak stress achieved during tensile deformation, but UTS alone does not account for the work hardening or softening ability with progressive straining. For a conventional tensile engineering stress-strain curve, strain hardening dominates in the uniform elongation region from yield stress (YS) to UTS; while geometrical softening dominates post-necking from UTS to failure, thereby representing a decrease in load-bearing ability [28]. Therefore, NSR based on UTS cannot distinguish between the effect of a notch on the part of the stress-strain curve before UTS and the notch effect on the part of the curve after UTS. For example, in **Fig. 1** (c), while uniform elongation is clearly higher in the un-notched specimen, careful observation reveals that the non-uniform ductility part is also more pronounced in the

un-notched specimen compared to the notched specimen. The curve of the notched specimen is marked by sharp geometrical softening in the non-uniform ductility region. Therefore, we sought to differentiate quantitatively between the strain hardening and geometrical softening contribution of the notch. The geometrical softening contribution of the notch was quantified by defining a geometrical softening factor ( $GSF_{\text{notch}}$ ) described by equation (2),

$$GSR = (\text{UTS} - \text{Fracture stress}) / (\text{Fracture strain} - \text{Uniform strain}) \quad (2a)$$

$$GSF_{\text{notch}} = GSR_{\text{notched}} / GSR_{\text{un-notched}} \quad (2b)$$

where GSR is the geometrical softening rate.

Similarly, a strain hardening factor ( $SHF_{\text{notch}}$ ) was calculated by equation (3).

$$NSHR = (\text{UTS}-\text{YS}) / \text{Plastic strain at UTS} \quad (3a)$$

$$SHF_{\text{notch}} = NSHR_{\text{notched}} / NSHR_{\text{un-notched}} \quad (3b)$$

where NSHR is the net strain hardening rate.

The ratio  $GSF_{\text{notch}}/SHF_{\text{notch}}$  then quantifies the relative contribution of the notch to strengthening in the uniform ductility regime and weakening in the non-uniform ductility regime. From the present un-notched curve and notched curve with reduced area (black and green, respectively),  $GSF_{\text{notch}}/SHF_{\text{notch}}$  ratio of 2.21 is obtained. This result indicates that the decrease in load-bearing ability after UTS due to the presence of a notch is 2.21 times higher than the strengthening rendered by the notch in the plastic regime up to UTS. By this approach, distinguishing why a material can undergo notch-strengthening (resulting in the stress-strain curve shifting upwards to higher stress), yet accelerate the onset of failure (resulting in much lower strain to failure) is easy. The importance of this approach can be realized by considering the fact that intuitively, a notch was always regarded as a weakness in the material, per se; which is, in the first place the reason why researchers investigated whether the notch effect of materials is strengthening or weakening, as Qu et al. appropriately presented the title of their paper as a question ("Notch Effect of Materials: Strengthening or Weakening?" [2]).

The conventional strain hardening rate ( $d\sigma/d\varepsilon$ ) curves obtained from the flow curves (true stress-strain curves) are also plotted in **Fig. 1** (d). The  $d\sigma/d\varepsilon$  curve for the notched specimen shows a more pronounced hump than the un-notched specimen. This more pronounced hump is attributed to higher twinning activity to accommodate high local plastic strain in the notched  $Al_{0.1}$ -HEA specimen. The activation of twinning to accommodate strain near the notch was confirmed from microstructural analysis of the failed notch-tensile specimen.

#### 3.2. Microstructural evolution in notch-tensile specimen of $Al_{0.1}$ -HEA

**Fig. 3** (a) shows a photograph of the failed notch-tensile specimen of  $Al_{0.1}$ -HEA marking the regions at which SEM-BSE characterization was

performed. Fig. 3 (b)–(g) show SEM-BSE images depicting various microstructural regimes on the gage length of the failed notch-tensile specimen as a function of distance from the notch. Clearly, approaching from the tensile gage region near the grip (far away from the notch) to the gage region in the vicinity of the notch not only shows different microstructural features but also progressively bears the signature of increasingly deformed material, thereby proving that deformation localization due to the presence of notch impacts the microstructural evolution in Al<sub>0.1</sub>-HEA. Fig. 3 (b) and (c) show the microstructure of the gage near the grip and at mid-gage locations, respectively. More slip bands are observed in the mid-gage than near the grip with a slight increase in surface roughness. However, a pronounced increase in surface roughness as observed in Fig. 3 (d) shows the highly deformed region near the notch. Further, the boundary of the strain localized region can be easily distinguished near the curvature of the notch (resulting from V-notch widening into a semi-circular shape), as depicted by the yellow dotted line in Fig. 3 (e). The distinctly higher deformation region with higher surface roughness (almost resembling a fracture surface) above the yellow line confirms that the deformation mechanism-induced microstructure is different in the strain localized region. Higher magnification images at the fracture tip near the notched region (Fig. 3 (f) and (g)) reveal characteristic thick deformation twin bands (some examples marked by yellow arrows in Fig. 3 (g)). Shear bands, surface roughness and micro-crack formation (examples of the latter are circled in red in Fig. 3 (g)) all reflect various concurrent mechanisms activated to accommodate the extremely high local strain at the notch and subsequent damage initiation.

The strain hardening curves in Fig. 1 (d) and the SEM-BSE imaging in Fig. 3 indicated that twinning induced plasticity is the vital mechanism for strain accommodation near the notch in Al<sub>0.1</sub>-HEA. Therefore, EBSD and TEM characterization were performed to verify the twin formation propensity near the notch (Fig. 4). The EBSD inverse pole figure (IPF) map in Fig. 4 (a) clearly depicts the formation of several twins within individual grains throughout the microstructure. The shape of the twins unambiguously reflects that these are deformation twins formed to accommodate the localized strain near the notch. The misorientation profile across lines 1 and 2 marked in Fig. 4 (a) are shown in Fig. 4 (b1) and (b2), respectively. They confirm that these are indeed twin

boundaries (60° misorientation angle peaks) and also provide information about twin thickness and twin density. Although twins with sub-micron lamellar thickness as well as > 1 μm thick twins are regularly observed in the microstructure, an important feature to note is that most of the twinned grains are characterized by repeated nucleation of the same variant. Since deformation twin nucleation is strongly dependent on the local stress state, the high frequency of twin nucleation sites can be attributed to local stress fluctuations in the strain localized vicinity of the notch. Additionally, there is also significant twin growth in the grains with high twin propensity, as confirmed from twin density measurements using ImageJ software. The twin densities in such grains, marked by lines 1 and 2 in Fig. 4 (a), are 27.1% and 38.1% area fraction of the grain.

The TEM images in Fig. 4 (c1-c2) also confirm that in addition to the twins captured by EBSD, fine nano-scale twins are also present near the notch. A few examples of these nanotwins are marked by yellow dotted lines in Fig. 4 (c2). Interestingly, these are actually secondary twins within a 1.3 μm thick primary twin marked by the red dotted lines. The importance of these extremely fine nanotwins is that they can cause exceptional increase in work hardening by acting as effective barriers to dislocation motion (resulting in reduced mean free path of dislocations) and due to dislocation-twin boundary interaction. Nanotwins effectively impede dislocation motion because high critical stresses are needed for dislocations to penetrate twin boundaries combined with the fact that a limited number of dislocations can be contained between two adjacent twin boundaries [29]. Komarasamy et al. earlier showed that significantly higher work hardening was obtained in Al<sub>0.1</sub>-HEA with nano-twins in the microstructure as compared to other low stacking fault energy materials that exhibited micron-sized twins [23]. Therefore, it is clear that the more pronounced hump in strain hardening curve of notch-tensile specimen of Al<sub>0.1</sub>-HEA (Fig. 1 (d)) is due to nano-scale twinning induced plasticity. Additionally, the high propensity for twin nucleation with substantial twin growth accounting for high twin fraction within individual grains (as confirmed from EBSD) indicates that deformation twinning is the dominant strain accommodation mechanism in the near-notch region. The stress triaxiality due to the presence of a notch introduces local stress concentrated twin nucleation sites. Since twinning induces a positive resolved shear stress at the twin front

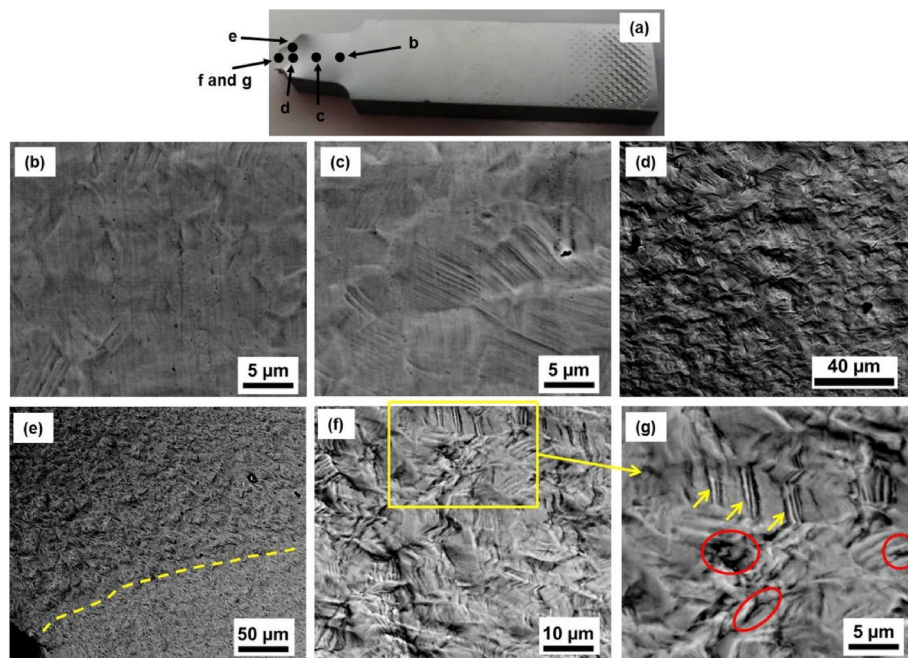


**Fig. 3.** (a) Photograph of a failed notch-tensile specimen of Al<sub>0.1</sub>-HEA marking the regions on gage length for which SEM-BSE images of microstructure are shown in (b) near the grip region, (c) mid-gage region, (d) near the notch, (e) at the curvature of the notch, and (f) and (g) at the fracture tip.

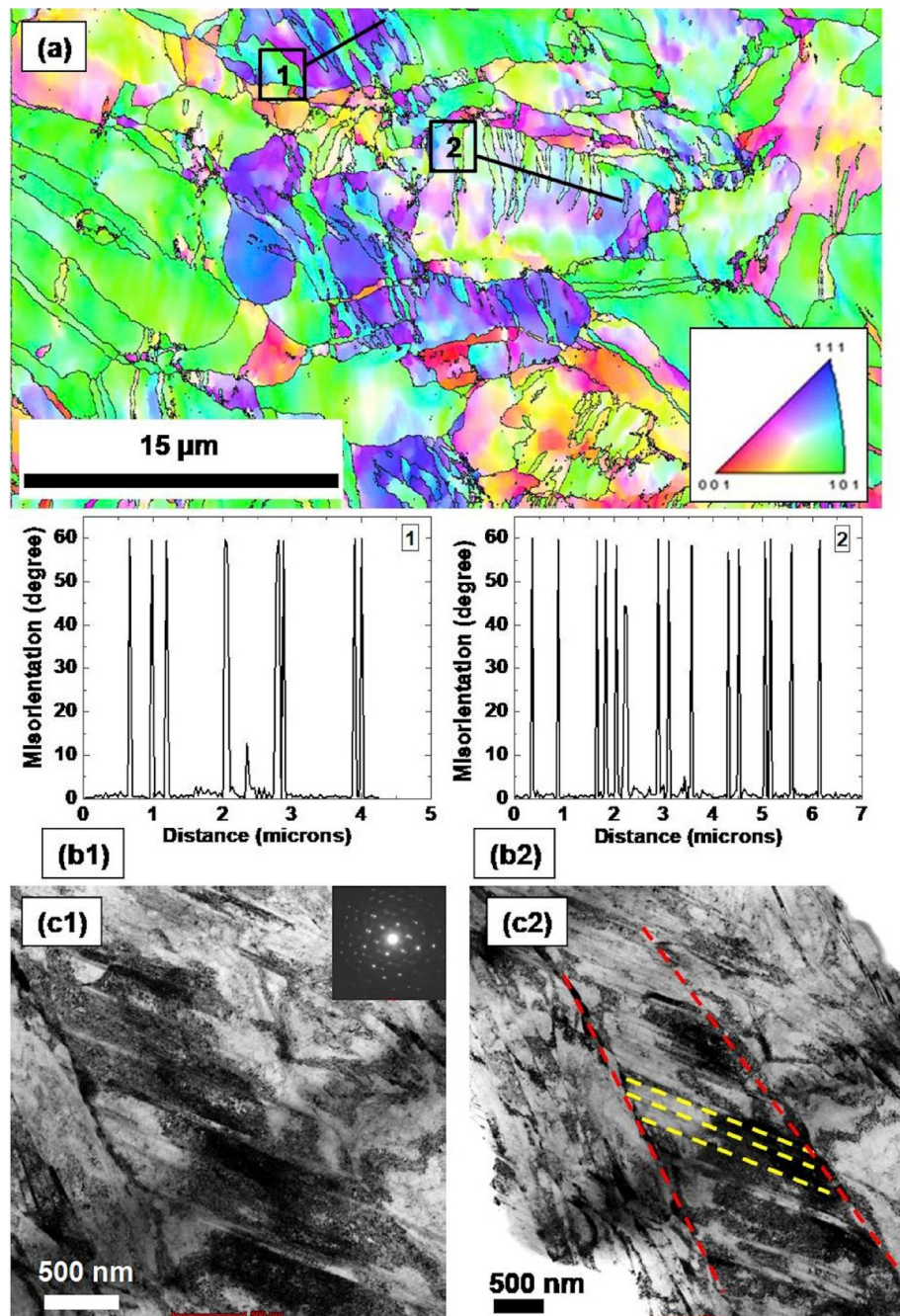


**Fig. 4.** (a) EBSD IPF map of the near-notch region in notch-tensile deformed specimen of  $\text{Al}_{0.1}\text{-HEA}$  showing deformation twins, (b1) misorientation profile across line 1 marked in (a) and (b2) misorientation profile across line 2 marked in (a), and (c1-c2) TEM characterization of nano-scale twinning in notch-tensile deformed specimen of  $\text{Al}_{0.1}\text{-HEA}$ . (The inset in (c1) shows diffraction pattern, while in (c2), the boundaries of a primary twin are marked by red dotted lines and nano-scale secondary twins within it are marked by yellow dotted lines).

but a negative resolved shear stress at the twin-matrix interface, the deformation twinning process inherently favors twin propagation but not lateral thickening of twins (twin growth) [30]. Instead, twin thickening is strongly dependent on the external applied stress, which provides the driving force for twin growth [30]. From this point of view, it is easy to appreciate why thick twin bands are observed near the notch in the present study. The stress triaxiality due to the notch enhances the impact of applied stress and therefore, considerable twin thickening occurs to plastically accommodate the high localized strain field in the vicinity of the notch.

### 3.3. Strain localization near the notch in $\text{Al}_{0.1}\text{-HEA}$

Plastic strain localization near the notch was measured and studied using DIC analysis. Fig. 5 (a) shows the successive frames showing the

axial strain development with local strain accumulation around the notch tip during the notch-tensile test of  $\text{Al}_{0.1}\text{-HEA}$ . Localized plastic deformation near the notch-pair (notches on either side) is visible through frames I-IX. Initially, notch widening occurs during stages I-III, wherein the V-shaped notches open up into semi-circular shape with increasing radius of curvature as strain increases. Stages IV-VI show clearly the gradual development of high local strain field in the tensile gage region between the pair of notches. With progressive straining in stages VII-IX, extremely high local strain develops in the vicinity of the notch pair along with crack initiation.

Fig. 5 (b) is an enlarged image of the DIC frame near failure strain (corresponding to stage IX) where cracks are observed at the notches on both sides. Exceptionally high local strain ( $\sim 180\%$ ) was obtained at the left notch where significant crack opening is also observed. The profile of this crack is presented in the left inset in Fig. 5 (b). While the crack on

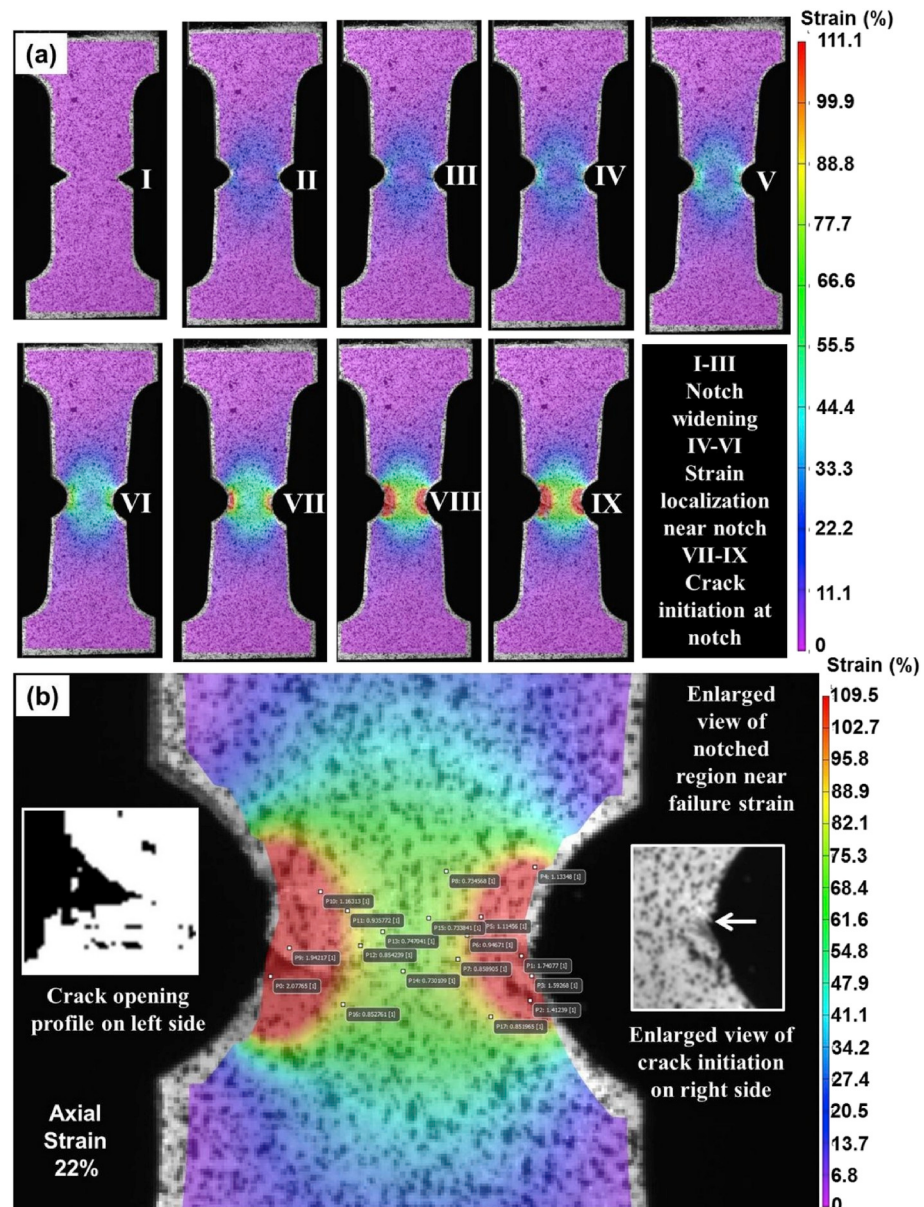


**Fig. 5.** DIC frames at (a) successive stages of notch-tensile test, and (b) enlarged view of notched region near the failure strain (at 22% axial strain) of Al<sub>0.1</sub>-HEA; insets in (b) show crack initiation at notch.

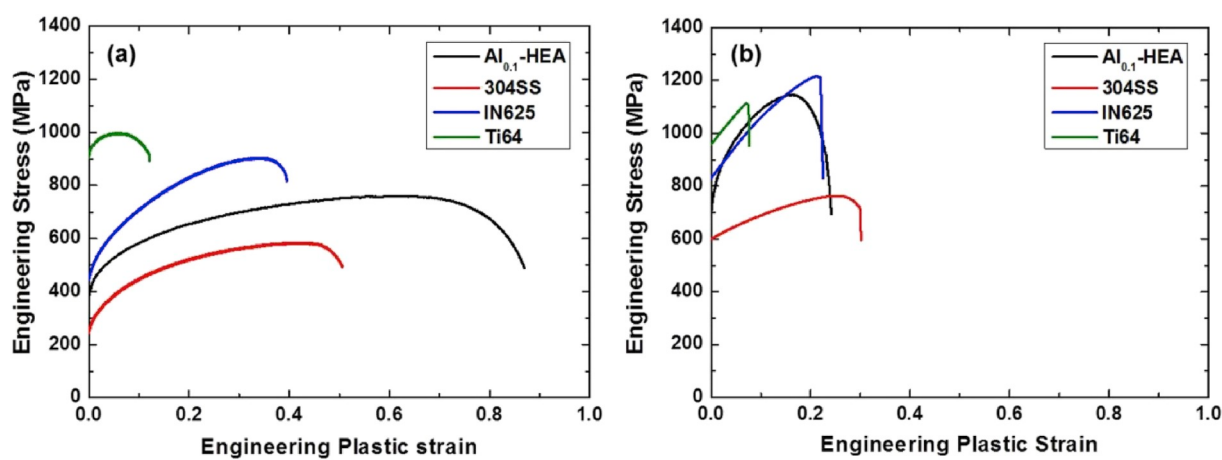


**Fig. 6.** Engineering stress-strain curves for (a) un-notched and (b) notched specimens of all four alloys in the present study.

the left notch already widened considerably, another crack initiated at the shoulder of the right notch, although it did not open up yet (white arrow in the right inset in Fig. 5 (b) points to the crack initiation site). The spread of the local strain field to the center of the gage (along the width of the specimen) is fairly uniform and radial (yellow and green regions in Fig. 5 (b)).

### 3.4. Comparison of $\text{Al}_{0.1}\text{-HEA}$ notch behavior with 304SS, IN625 and Ti64 alloys

Fig. 6 shows comparison of the tensile response of  $\text{Al}_{0.1}\text{-HEA}$  with three other conventional alloys (304SS, IN625 and Ti64) in the un-notched and notched conditions. The quantification of notch effects using NSR and  $\text{GSF}_{\text{notch}}/\text{SHF}_{\text{notch}}$  ratio are summarized in Table 1. The engineering stress-strain curves in Fig. 6(a-b) show that in the notched condition, UTS of  $\text{Al}_{0.1}\text{-HEA}$  (1147.4 MPa) is closer to IN625 (1216.3 MPa) than 304SS (762.7 MPa); while in the un-notched condition, UTS of  $\text{Al}_{0.1}\text{-HEA}$  (760.1 MPa) is mid-way between 304SS (584.8 MPa) and IN625 (905.2 MPa). Also, Table 1 shows that  $\text{Al}_{0.1}\text{-HEA}$  has higher NSR of 1.51 than 304SS, IN625 and Ti64 (1.30, 1.34 and 1.12, respectively). This confirms that the notch-strengthening effect in  $\text{Al}_{0.1}\text{-HEA}$  is stronger compared to the three conventional materials.

Table 1 also shows that  $\text{Al}_{0.1}\text{-HEA}$  has the lowest  $\text{GSF}_{\text{notch}}/\text{SHF}_{\text{notch}}$  ratio of 2.21, compared to 304SS, IN625 and Ti64 (4.85, 17.65 and 9.28, respectively). Note that the value of  $\text{GSF}_{\text{notch}}/\text{SHF}_{\text{notch}}$  of  $\text{Al}_{0.1}\text{-HEA}$  is closer to 304SS compared to IN625. The high  $\text{GSF}_{\text{notch}}/\text{SHF}_{\text{notch}}$  value for IN625 explains the steep drop in the notch-tensile engineering stress-strain curve of this material (Fig. 6 (b)), signifying that although IN625 has a fairly good notch-strengthening effect (NSR = 1.34), post-UTS deformation is marked by strong decrease in load bearing ability due to the presence of a notch. On the other hand,  $\text{Al}_{0.1}\text{-HEA}$  combines good notch-strengthening (NSR = 1.51) with reasonable load bearing capability post-UTS. In short,  $\text{Al}_{0.1}\text{-HEA}$  combines attributes of both IN625 and 304SS to provide better notch-tensile response than what would be expected merely from its un-notched tensile properties.

The notch-strengthening and associated fracture toughness of the  $\text{Al}_{0.1}\text{-HEA}$  is related to classical high-entropy effects that influence the plastic deformation of the HEA. The possible rate-controlling mechanisms include local nano-scale chemical heterogeneities such as short range ordering or clusters or the effect of individual solute atoms as obstacles [31]. HEAs have a high probability that the attraction between specific atoms (e.g. 2 out of 5 elements) is higher than the others. This results in “co-clustering” of these elements, which reduces the free energy significantly [32]. Since the enthalpy of cluster formation is a more local quantity than the entropy of mixing (the latter is a quantity averaging over a volume containing many atoms), the local effect of enthalpy of cluster formation is stronger, creating nano-scale heterogeneities that influence the plastic deformation. Also, the inherent ductility and hence, the fracture toughness of HEAs is dependent on the number of d and s electrons per atom [31]. These various factors contributed to the unconventional notch-strengthening effect observed in  $\text{Al}_{0.1}\text{-HEA}$  in the present study.

The grain sizes of the  $\text{Al}_{0.1}\text{-HEA}$ , 304SS, IN625 and Ti64 alloys in the present study are  $4.6 \pm 1.0 \mu\text{m}$ ,  $44.7 \pm 6.3 \mu\text{m}$ ,  $43.2 \pm 4.5 \mu\text{m}$  and  $7.6 \pm 1.1 \mu\text{m}$ , respectively (EBSD IPF maps shown in Fig. 7(a-d)). Although the impact of grain size requires further study and is not included in this paper, it is worthwhile to discuss its importance. The influence of grain

size or notch size/grain size ratio on the notch-sensitivity in any alloy is unique to that particular alloy. In general, the notch-sensitivity increases with decrease in grain size, while increasing the size of the microstructure makes the notch less and less significant [33]. Also, finer grains increase the crack growth resistance [34]. Other important factors are the crystal structure of constituent phases in the microstructure and associated deformation mechanisms. For instance, if the alloy undergoes twinning, the effective grain size reduction caused by twinning would induce the grain refinement effect on notch-sensitivity indirectly. Further, the definition of the aforementioned “size of the microstructure” that is coarse enough to cause significant difference in notch-sensitivity depends on the specific alloy. Lorenzino and Navarro discussed increase in notch-sensitivity with decrease in grain size in 1050 grade Al-alloy by comparing grain sizes of the order of  $400 \mu\text{m}$ ,  $1.4 \text{ mm}$ ,  $3.5 \text{ mm}$  and  $9.7 \text{ mm}$  [33]. On the other hand, Kanemaru et al. found different notch-sensitivity and crack growth resistance for  $6.5 \mu\text{m}$  and  $20 \mu\text{m}$  grain-sized microstructures in carbon steel [34]. Interestingly, the behavior of polycrystalline ice is opposite to the aforementioned Al-alloy or carbon steel. Nixon and Schulson discussed that polycrystalline ice exhibits notch-strengthening for grain size  $>5 \text{ mm}$ , while the notch-strengthening effect diminishes with decrease in grain size and disappears at grain size  $<3 \text{ mm}$  [35]. Therefore, the influence of grain size on notch-strengthening effect is a complicated subject and its effect on the present alloys is open for future investigations.

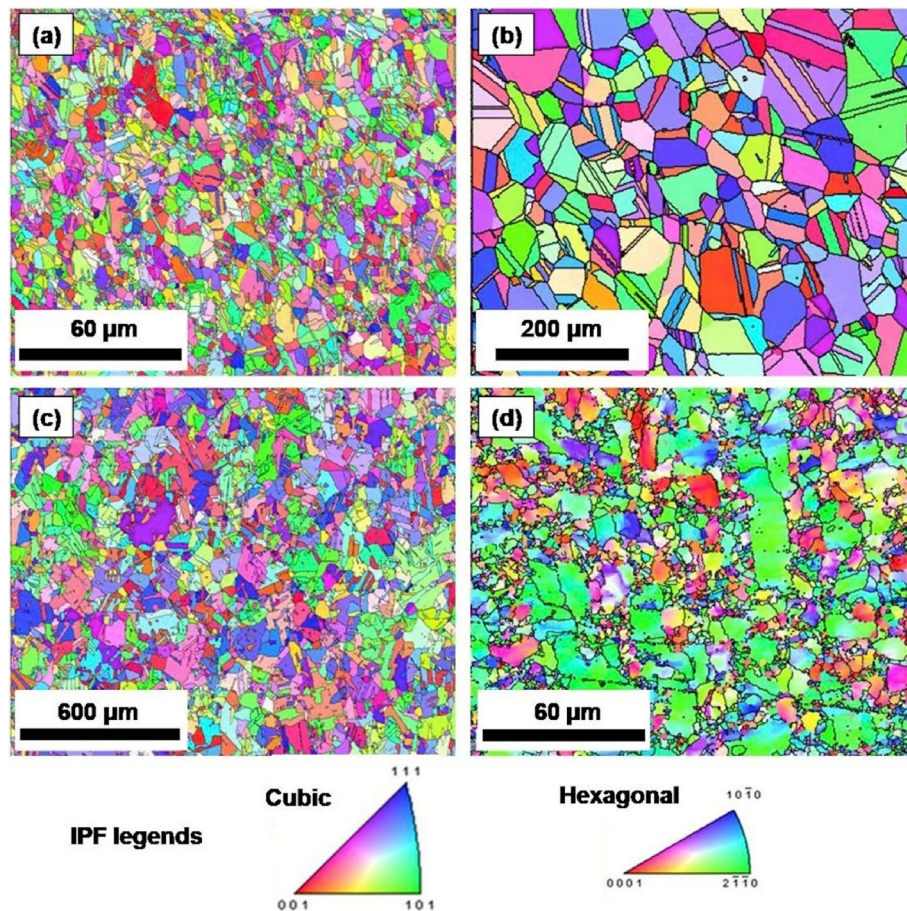
Finally, the microstructure and crystal structure of constituent phases also influence the notch-tensile behavior of these alloys. In the present study,  $\text{Al}_{0.1}\text{-HEA}$ , 304SS and IN625 have f.c.c. crystal structure.  $\text{Al}_{0.1}\text{-HEA}$  and IN625 show the presence of a few annealing twins in the starting microstructure (Fig. 7 (a) and (c), respectively); and the starting microstructure of 304SS has a high density of annealing twins (Fig. 7 (b)). On the other hand, Ti64 has predominantly hexagonal close packed (h.c.p.) structured  $\alpha$ -Ti phase in the microstructure interspersed with some  $\beta$ -Ti phase with body centered cubic (b.c.c.) crystal structure. The h.c.p. crystal structure has lower symmetry and hence, provides fewer active slip systems than the f.c.c. crystal structure, due to which the former is a less ductile phase compared to the latter. Therefore, Ti64 has high strength but low ductility compared to the other three alloys. Now, the primary influence of microstructure on the notch-tensile behavior of these alloys is related to the crack growth resistance which influences the ductility and toughness in notch-tensile test. The presence of  $\beta$  (b.c.c.) phase distributed within the predominantly  $\alpha$  (h.c.p.) microstructure, especially at the grain boundaries, is detrimental because the strain mismatch at the phase interfaces could result in probable sites for crack nucleation. Similarly, annealed IN625 is known to possess precipitates, intermetallic phases or carbides at grain boundaries that are detrimental to its ductility and toughness [36,37]. This is the possible reason why IN625 showed the highest  $\text{GSF}_{\text{notch}}/\text{SHF}_{\text{notch}}$  value of 17.65 (Table 1), accounting for the steep drop in engineering stress-strain curve after UTS (Fig. 6 (b)).

Fig. 8 shows the DIC frame near failure strain for IN625, 304SS and Ti64 for comparison of strain localization and damage in the vicinity of the notch with respect to that observed in  $\text{Al}_{0.1}\text{-HEA}$ . Clearly, the difference in deformation behavior at the notch is evident from the different mode or extent of opening of the V-notch at higher strain. Ti64 retained the V-notch shape although the notch became wider. In contrast,  $\text{Al}_{0.1}\text{-HEA}$ , 304SS and IN625 all showed opening up of the V-notch into semi-circular shape.  $\text{Al}_{0.1}\text{-HEA}$  and 304SS showed larger radius of curvature; i.e., the notch opened up wider than IN625. The extent of notch widening is clearly determined by the strength and ductility of the material. Hence, Ti64 shows least notch widening, followed by IN625; while 304SS and  $\text{Al}_{0.1}\text{-HEA}$  show greater notch widening.

Strain localization near the notch and its spread with distance from the notch tip (visible from DIC strain mapping) are different for various materials. The shape of the strain field depends on the nature and the amount of notch widening. The high local strain region at the tip of the

**Table 1**  
Quantification of notch effects in the present materials.

Material	NSR	$\text{GSF}_{\text{notch}}/\text{SHF}_{\text{notch}}$
$\text{Al}_{0.1}\text{-HEA}$	1.51	2.21
304SS	1.30	4.85
IN625	1.34	17.65
Ti64	1.12	9.28



**Fig. 7.** EBSD IPF maps showing the initial microstructures of (a) Al<sub>0.1</sub>-HEA (b) 304SS (c) IN625 and (d) Ti64.

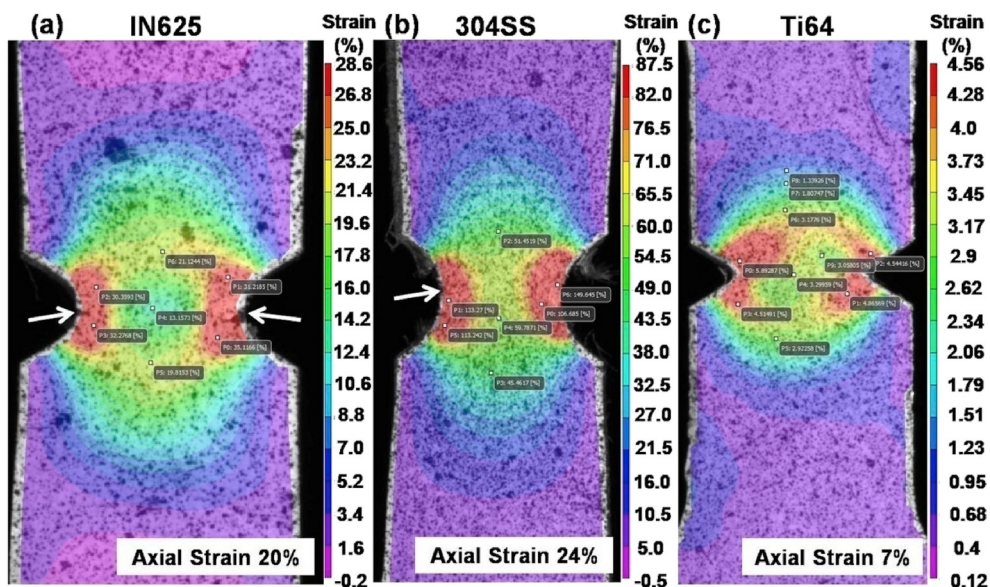


**Fig. 8.** DIC frame near failure strain for notched tensile test of (a) Inconel 625, (b) 304 stainless steel and (c) Ti-6Al-4V for comparison. (Note: White arrows denote the crack initiation sites).

notch (red) is elliptical along the curvature of the widened notch (extending radially from the original tip of the notch) for Al<sub>0.1</sub>-HEA (Fig. 5 (b)), IN625 (Fig. 8 (a)) and 304SS (Fig. 8 (b)). In contrast, Ti64 shows a divergent red strain field centered at the tip of the notch

(both sides of the specimen). Instead of spreading radially, the red region extends directionally perpendicular to the two angular arms of the V-notch (Fig. 8 (c)). As a result, the red region spreads to a smaller distance at the notch tip but to a greater distance perpendicular to the

inclined sides of the (widened) notch. Wang and Gao defined the formation of “two narrowing sectors and an expanding sector” that constitute the notch tip field [38]. Specifically, the red region of the strain field shows characteristic “narrowing” and “expanding” sectors only in Ti64 (Fig. 8 (c)). In fact, the two positionally “narrowing” sectors at the inclined sides of the notch are larger; while the sector at the notch tip, which by definition based on location would be the “expanding” sector, is smaller. On the other hand, Al<sub>0.1</sub>-HEA, 304SS and IN625 show uniformly-sized “expanding” and “narrowing” sectors. As a result, the entire strain field distribution is also different in different alloys. Ti64 shows an asymmetric barreled strain field compared to the other three alloys. Also, the distinct circular low strain region (light blue/green) between the red regions in Ti64 and IN625 (although the strain field of the latter is not as barreled as Ti64) indicates clearly that the high local strain field due to the notch is more concentrated at the notch in Ti64 and IN625 (which also show lower notch-widening), than Al<sub>0.1</sub>-HEA and 304SS that show symmetric, uniform strain field spreading to the tensile gage away from the notch.

Graff et al. discussed that in Al-Cu alloys, smooth U-notched specimens tend to fracture in the middle of the deformed zone, while sharp U-notched specimens tend to fracture at the notches [39]. Their findings thus confirm that the curvature of the notch, induced by nature of notch widening, determines strain localization distribution and the propensity for crack initiation in the present materials. Since the V-notch remains sharper even after widening in Ti64, the high local strain field is asymmetric and more concentrated at the notch. IN625 also has smaller radius of curvature of the widened notch (sharper); hence, lower local strain is developed in the middle of the deformed zone (center of specimen is light blue in Fig. 8 (a)) than 304SS (Fig. 8 (b)) and Al<sub>0.1</sub>-HEA (Fig. 5 (b)) (green zone spreads to the middle for the latter two).

The DIC frames near failure strain in Fig. 8 for IN625, 304SS and Ti64 also capture crack formation at the notch in these materials in comparison with Al<sub>0.1</sub>-HEA (Fig. 5 (b)). Interestingly, while pronounced crack growth was observed in Al<sub>0.1</sub>-HEA, cracks are observed at the notch in IN625 and 304SS (marked by white arrows in Fig. 8 (a) and (b), respectively), but not in Ti64. This is surprising, since Ti64 is a less ductile alloy than the other three alloys (which would lead us to expect that crack formation should occur more readily in this Ti64). First impressions might suggest that this is due to the lower absolute axial strain levels in Ti64 compared to the other materials (Fig. 8). However, this difference in strain levels is due to the inherent strength-ductility of the respective alloys. Note that, whatever be the strain levels, comparison is made between and among all the alloys near their respective failure strain. Therefore, crack formation probability would not depend on strain level alone. Moiseenko et al. discussed the effect of notch shape on strain localization in steel, using U, V and I-shaped notches [40]. These authors confirmed that the shape of the notch influences stress relaxation near the concentrator by developing different force moment distributions. I-notch providing largest relaxation capacity gives rise to lower scale of stress near the stress riser. V-notch provides greater stress relaxation than U-notch. In the present study, a V-notch was used in all the four alloys but the shape of the notch after notch-widening was different. Therefore, a widened V-notch that still remains V-shaped (as happens in Ti64) would provide more stress relaxation than a widened notch that has become semi-circular (observed in Al<sub>0.1</sub>-HEA, 304SS and IN625). Thus, more stress relaxation occurs in Ti64. Now, crack formation is more strongly dependent on stress state (triaxiality) than local strain distribution. This explains the apparent ambiguity as to why cracks are not observed in Ti64 in Fig. 8 (c). Of course, this does not mean cracks did not form in Ti64 when the alloy failed. The DIC observations simply confirm that crack formation and growth process leading to failure were more gradual in Al<sub>0.1</sub>-HEA, IN625 and 304SS. For the same reason, crack formation was captured in multiple frames in Al<sub>0.1</sub>-HEA (VII-IX in Fig. 5 (a)). The ability of these three alloys to accommodate local damage due to crack propagation by crack energy absorption or dissipation is higher than Ti64. The latter three alloys

show higher propensity for stable crack growth (that is associated with plastic collapse instead of being superseded by catastrophic failure [41]). On the other hand, unstable crack propagation and crack growth rate in Ti64 is definitely higher, and results in sudden failure after crack initiation.

### 3.5. Finite element modeling of stress distribution around the notch

Finite element modeling was performed to obtain the equivalent plastic strain and von Mises stress distribution around the notch for all the four alloys (Al<sub>0.1</sub>-HEA, 304SS, IN625 and Ti64). Fig. 9 shows the fit of the stress-strain curves obtained from the finite element model to the corresponding experimental curves for all four alloys. Since damage modeling was not incorporated in the finite element model, the model is incapable of determining the post uniform elongation tensile behavior after crack initiation. Therefore, for both experimental and simulation curves in Fig. 9, only the uniform plastic part is shown to depict the degree of match between the two (for each alloy). The reasons for some mismatch between the experimental and simulated stress-strain curves (e.g. in Ti64) can be summarized as follows. First of all, a notch-tensile test is inherently different from a regular quasi-static tensile test in terms of stress-state and material behavior with respect to hardening and plastic deformability, onset of plastic instability and propensity for cracking and failure. Therefore, the exact hardening response that the specimens actually underwent during experimental testing is unknown and possibly, there was considerable deviation from known conventional hardening laws (or the hardening response as a function of strain was irregular). In line with this, the second factor is that a Johnson-Cook model [42] type power law fit of the experimental data was used to include the material response in the finite element simulation. The mismatch may be attributed to the fact that at the maximum possible refinement achieved by iteration, a power law simply was not enough to precisely fit the experimental hardening response, considering that it was a notch-tensile test. Also, a better match is possible if a material model that includes microstructural aspects like grain size and orientation (crystallographic texture) and hardening of slip and twin mechanisms, is incorporated. Third, the notch-tensile tests were performed within the limits of experimental error. It is possible that slight imprecision associated with experimental testing contributed to the mismatch between simulated and experimental curves.

The equivalent plastic strain distributions and von Mises stress distributions at strains near the failure in each material are shown in Fig. 10 (a1-a4) and (b1-b4), respectively. Clearly, the simulation confirms the different extent of notch widening observed experimentally in the different alloys. Also, the equivalent plastic strain distributions around the notch (Fig. 10 (a1-a4) obtained from simulation) are similar to the experimental axial strain distribution maps from DIC (Fig. 5 (b) and 8). Al<sub>0.1</sub>-HEA and 304SS show uniform, radial spread of the local strain field from the expanding sector at the tip of the notch. On the other hand, IN625 and Ti64 show strain field spreading along positionally “narrowing” sectors. Further, the stress distributions in Fig. 10 (b1-b4) verify the alloy dependence of notch effect on strain localization observed experimentally in Fig. 5 (b) and 8. Lower stress is observed in the middle of the deformed zone (center of the specimen in the notched region) in Ti64 and IN625 compared to Al<sub>0.1</sub>-HEA and 304SS (similar to the strain field discussed earlier). The stress concentration also spreads along the positionally “narrowing” sectors in Ti64 and IN625, while it expands radially from the tip of the notch in Al<sub>0.1</sub>-HEA and 304SS. Thus, the simulation validates the inference drawn from DIC experiment, that the type of material has a strong influence on the strain localization and stress state in notched specimens. Also, Fig. 10 (b1-b4) show that higher stress is accommodated at the tip of the notch in Al<sub>0.1</sub>-HEA, 304SS and IN625 than Ti64. This confirms that crack formation in Ti64 occurs more readily at lower stress level than the other three alloys, since Ti64 is less ductile; and that, crack formation is strongly related to the stress state.

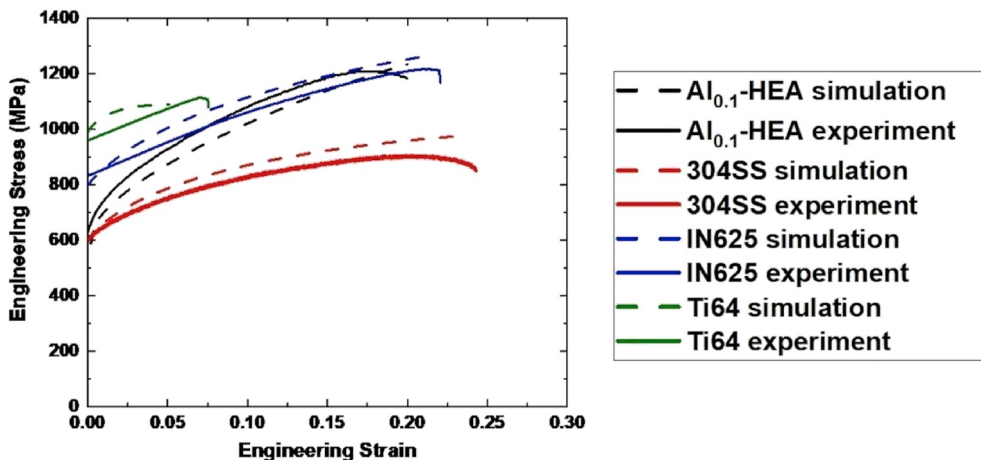


**Fig. 9.** Fit of the simulated stress-strain curves from finite element modeling to the corresponding experimental curves for  $\text{Al}_{0.1}\text{-HEA}$ , 304SS, IN625 and Ti64.

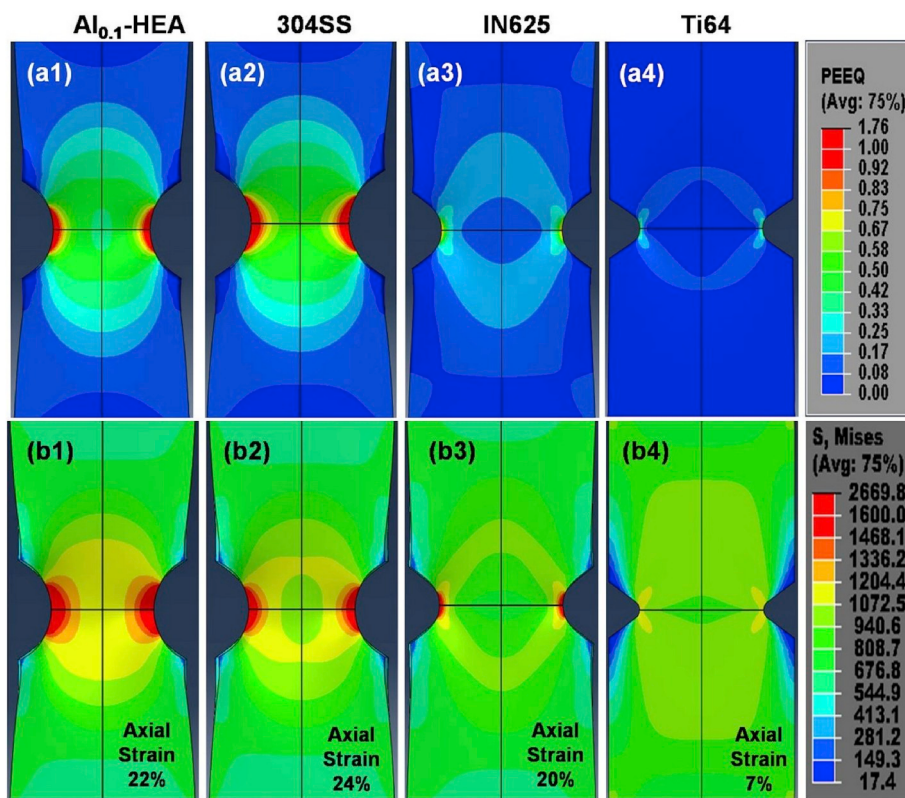


**Fig. 10.** (a1-a4) Equivalent plastic strain distributions and (b1-b4) von Mises stress distributions around the notch for all the four alloys at strains near the failure in each material.

#### 4. Summary

The notch-tensile behavior of  $\text{Al}_{0.1}\text{CrFeCoNi}$  HEA was investigated and compared with 304 stainless steel, Inconel 625 and Ti-6Al-4V alloys using a V-notch geometry. Although all these alloys exhibited notch-strengthening,  $\text{Al}_{0.1}\text{CrFeCoNi}$  HEA showed notch-strength ratio of 1.51, which was higher than the three conventional alloys. Quantitative analysis of the stress-strain curves also revealed that  $\text{Al}_{0.1}\text{CrFeCoNi}$  HEA exhibited UTS close to Inconel 625 in notch-tensile test combined with post-UTS load bearing ability similar to 304 stainless steel (that is more ductile than Inconel 625). Microstructural analysis showed that the high local strain in the vicinity of the notch was accommodated by twinning induced plasticity in  $\text{Al}_{0.1}\text{CrFeCoNi}$  HEA.

DIC experiment and finite element modeling revealed that the inherent strength-ductility of each material influenced notch widening and associated localized strain field and stress distribution. Therefore,  $\text{Al}_{0.1}\text{CrFeCoNi}$  HEA shows good notch-tensile behavior with the combined attributes of 304 stainless steel and Inconel 625. Also,  $\text{Al}_{0.1}\text{CrFeCoNi}$  HEA has higher propensity for stable crack growth and local damage accommodation by crack energy absorption or dissipation than Ti-6Al-4V alloy.

#### Author contributions

Subhasis Sinha: Conceived and designed the analysis, Collected the data, Contributed data or analysis tools, Performed the analysis, Wrote

the paper. Mageshwari Komarasamy: Conceived and designed the analysis, Collected the data, Contributed data or analysis tools. Tianhao Wang: Conceived and designed the analysis, Collected the data, Contributed data or analysis tools. Ravi Sankar Haridas: Conceived and designed the analysis, Performed the analysis. Priyanka Agrawal: Collected the data, Performed the analysis. Shivakant Shukla: Collected the data, Performed the analysis. Saket Thapliyal: Collected the data. Michael Frank: Collected the data. Rajiv S. Mishra: Conceived and designed the analysis, Wrote the paper.

## Declaration of competing interest

The authors have no conflict of interest.

## Acknowledgments

The work was performed under the cooperative agreement of University of North Texas with the Army Research Laboratory (W911NF-18-2-0067). Materials Research Facility at University of North Texas is acknowledged for allowing access to microscopy facilities. The authors thank Dr. Jeffrey T. Lloyd at the Army Research Laboratory for providing valuable insight during discussions.

## References

- [1] Z. Leng, J. Zhang, J. Sun, H. Shi, S. Liu, L. Zhang, M. Zhang, R. Wu, Notch tensile behavior of extruded Mg–Y–Zn alloys containing long period stacking ordered phase, Mater. Des. 56 (2014) 495–499, <https://doi.org/10.1016/j.matdes.2013.11.035>.
- [2] R. Qu, P. Zhang, Z. Zhang, Notch effect of materials: strengthening or weakening? J. Mater. Sci. Technol. 30 (2014) 599–608, <https://doi.org/10.1016/j.jmst.2014.04.014>.
- [3] A.M. Agogino, Notch effects, stress state, and ductility, J. Eng. Mater. Technol. 100 (1978) 349–355, <https://doi.org/10.1115/1.3443503>.
- [4] X. Lei, C. Li, X. Shi, X. Xu, Y. Wei, Notch strengthening or weakening governed by transition of shear failure to normal mode fracture, Sci. Rep. 5 (2015), <https://doi.org/10.1038/srep10537>, 10537–1–10537–10.
- [5] B. Swaminathan, J. Lambros, H. Sehitoglu, Digital image correlation study of mechanical response of nickel superalloy Hastelloy X under thermal and mechanical cycling: uniaxial and biaxial stress states, J. Strain Anal. 49 (2014) 233–243, <https://doi.org/10.1177/0309324713503959>.
- [6] D. Lindner, F. Mathieu, F. Hild, O. Allix, C.H. Minh, On the evaluation of stress triaxiality fields in a notched titanium alloy sample via integrated, J. Appl. Mech. 82 (2015), <https://doi.org/10.1115/1.4030457>, 4030457–1–4030457–13.
- [7] G.N. Morscher, R. Maxwell, Monitoring tensile fatigue crack growth and fiber failure around a notch in laminate SiC/Si composites utilizing acoustic emission, electrical resistance, and digital image correlation, J. Euro. Cer.Soc. 39 (2019) 229–239, <https://doi.org/10.1016/j.jeuceramsoc.2018.08.049>.
- [8] M. Štamborská, M. Kvíčala, M. Losertová, Identification of the mechanical properties of high-strength steel using digital image correlation, Adv. Mater. Res. 980 (2014) 122–126, <https://doi.org/10.4028/www.scientific.net/AMR.980.122>.
- [9] T. Wu, M. Coret, A. Combescure, Strain Localisation and Damage Measurement by Full 3D Digital Image Correlation: Application to 15-SPH Stainless steel, Wiley-Blackwell, 47, 2011, pp. 49–61, <https://doi.org/10.1111/j.1475-1305.2008.00600.x>, 1.
- [10] C.C. Roth, D. Mohr, Ductile fracture experiments with locally proportional loading histories, Int. J. Plast. 79 (2016) 328–354, <https://doi.org/10.1016/j.ijplas.2015.08.004>.
- [11] T. Matsuno, C. Teodosiu, D. Maeda, A. Uenishi, Mesoscale simulation of the early evolution of ductile fracture in dual-phase steels, Int. J. Plast. 74 (2015) 17–34, <https://doi.org/10.1016/j.ijplas.2015.06.004>.
- [12] M.B. Gorji, D. Mohr, Micro-tension and micro-shear experiments to characterize stress-state dependent ductile fracture, Acta Mater. 131 (2017) 65–76, <https://doi.org/10.1016/j.actamat.2017.03.034>.
- [13] C.C. Roth, D. Mohr, Effect of strain rate on ductile fracture initiation in advanced high strength steel sheets: experiments and modeling, Int. J. Plast. 56 (2014) 19–44, <https://doi.org/10.1016/j.ijplas.2014.01.003>.
- [14] V. Granados-Alejo, C. Rubio-González, C.A. Vázquez-Jiménez, J.A. Banderas, G. Gómez-Rosas, Influence of specimen thickness on the fatigue behavior of notched steel plates subjected to laser shock peening, Opt. Laser. Technol. 101 (2018) 531–544, <https://doi.org/10.1016/j.optlastec.2017.12.011>.
- [15] L. Cao, D. Bürger, P. Wollgramm, K. Neuking, G. Eggeler, Testing of Ni-base superalloy single crystals with circular notched miniature tensile creep (CNMTC) specimens, Mater. Sci. Eng. A 712 (2018) 223–231, <https://doi.org/10.1016/j.msea.2017.11.102>.
- [16] U. Roy, H. Roy, H. Daoud, U. Glatzel, K.K. Ray, Fracture toughness and fracture micromechanism in a cast AlCoCrCuFeNi high entropy alloy system, Mater. Lett. 132 (2014) 186–189, <https://doi.org/10.1016/j.matlet.2014.06.067>.
- [17] M. Seifi, D. Li, Z. Yong, P.K. Liaw, J.J. Lewandowski, Fracture toughness and fatigue crack growth behavior of as-cast high-entropy alloys, J. Occup. Med. 67 (2015) 2288–2295, <https://doi.org/10.1007/s11837-015-1563-9>.
- [18] K.V.S. Thurston, B. Gludovatz, A. Hohenwarter, G. Laplanche, E.P. George, R.O. Ritchie, Effect of temperature on the fatigue-crack growth behavior of the high-entropy alloy CrMnFeCoNi, Intermetallics 88 (2017) 65–72, <https://doi.org/10.1016/j.intermet.2017.05.009>.
- [19] S.-P. Wang, E. Ma, J. Xu, Notch fracture toughness of body-centered-cubic (TiZrNbTa)–Mo high-entropy alloys, Intermetallics 103 (2018) 78–87, <https://doi.org/10.1016/j.intermet.2018.10.008>.
- [20] Z. Lyu, X. Fan, C. Lee, S.-Y. Wang, R. Feng, P.K. Liaw, Fundamental understanding of mechanical behavior of high-entropy alloys at low temperatures: a review, J. Mater. Res. 33 (2018) 2998–3010, <https://doi.org/10.1557/jmr.2018.273>.
- [21] G. Bi, Y. Chew, F. Weng, Z. Zhu, F.L. Ng, B.Y. Lee, Process study and characterization of properties of FeCrNiMnCo high-entropy alloys fabricated by laser-aided additive manufacturing, Proc. SPIE 10813, Adv. Laser Process. Manufac. II (12 Nov. 2018), 108130V, <https://doi.org/10.1117/12.2502272>.
- [22] N. Kumar, M. Komarasamy, P. Nelaturu, Z. Tang, P.K. Liaw, R.S. Mishra, Friction stir processing of a high entropy alloy Al<sub>0.1</sub>CoCrFeNi, J. Occup. Med. 67 (2015) 1007–1013, <https://doi.org/10.1007/s11837-015-1385-9>.
- [23] M. Komarasamy, N. Kumar, Z. Tang, R.S. Mishra, P.K. Liaw, Effect of microstructure on the deformation mechanism of friction stir-processed Al<sub>0.1</sub>CoCrFeNi high entropy alloy, Mater. Res. Lett. 3 (2015) 30–34, <https://doi.org/10.1080/21663831.2014.958586>.
- [24] D. Choudhuri, M. Komarasamy, V. Ageh, R.S. Mishra, Investigation of plastic deformation modes in Al<sub>0.1</sub>CoCrFeNi high entropy alloy, Mater. Chem. Phys. 217 (2018) 308–314, <https://doi.org/10.1016/j.matchemphys.2018.05.050>.
- [25] Y.F. Shen, X.X. Li, X. Sun, Y.D. Wang, L. Zuo, Twinning and martensite in a 304 austenitic stainless steel, Mater. Sci. Eng. A 552 (2012) 514–522, <https://doi.org/10.1016/j.msea.2012.05.080>.
- [26] M. Vanderhasten, L. Rabet, B. Verlinden, Deformation mechanisms of Ti-6Al-4V during tensile behavior at low strain rate, JMEPEG 16 (2007) 208–212, <https://doi.org/10.1007/s11665-007-9033-3>.
- [27] M.M. de Oliveira, A.A. Couto, G.F.C. Almeida, D.A.P. Reis, N.B. de Lima, R. Baldan, Mechanical behavior of Inconel 625 at elevated temperatures, Metals 9 (2019), <https://doi.org/10.3390/met9030301>, 301–1–301–13.
- [28] G.E. Dieter, Mechanical Metallurgy, SI Metric, Ed., McGraw-Hill Book Company, London, 1988, pp. 275–292.
- [29] L.L. Shaw, J. Villegas, J.-Y. Huang, S. Chen, Strengthening via deformation twinning in a nickel alloy, Mater. Sci. Eng. A 480 (2008) 75–83.
- [30] M. Arul Kumar, A.K. Kanjarla, S.R. Niezgoda, R.A. Lebensohn, C.N. Tome, Numerical study of the stress state of a deformation twin in magnesium, Acta Mater. 84 (2015) 349–358.
- [31] S.-P. Wang, E. Ma, J. Xu, Notch fracture toughness of body-centered-cubic (TiZrNbTa)–Mo high-entropy alloys, Intermetallics 103 (2018) 78–87, <https://doi.org/10.1016/j.intermet.2018.10.008>.
- [32] S.I. Hong, J. Moon, S.K. Hong, H.S. Kim, Thermally activated deformation and the rate controlling mechanism in CoCrFeMnNi high entropy alloy, Mater. Sci. Eng. A 682 (2017) 569–576, <https://doi.org/10.1016/j.msea.2016.11.078>.
- [33] P. Lorenzino, A. Navarro, Grain size effects on notch sensitivity, Int. J. Fatigue 70 (2015) 205–215, <https://doi.org/10.1016/j.ijfatigue.2014.09.012>.
- [34] T. Kanemaru, K. Kawagoishi, E. Kondo, Q.Y. Wang, Y. Ohzono, Influence of grain size on notch sensitivities in fatigue of carbon steel, Key Eng. Mater. 385–387 (2008) 197–200, <https://doi.org/10.4028/www.scientific.net/KEM.385-387.197>.
- [35] W.A. Nixon, E.M. Schulson, A notch-strengthening effect in fresh-water ice, J. Glaciol. 36 (1990) 107–111, <https://doi.org/10.3189/S0022143200005621>.
- [36] P. Petrzak, K. Kowalski, M. Blicharski, Analysis of phase transformations in Inconel 625 alloy during annealing, Acta Phys. Pol. A 130 (2016) 1041–1044, <https://doi.org/10.12693/APhysPolA.130.1041>.
- [37] G. Marchese, S. Parizia, M. Rashidi, A. Saboori, D. Manfredi, D. Ugues, M. Lombardi, E. Hryha, S. Biamino, The role of texturing and microstructure evolution on the tensile behavior of heat-treated Inconel 625 produced via laser powder bed fusion, Mater. Sci. Eng. A 769 (2020), <https://doi.org/10.1016/j.msea.2019.138500>, 138500–138500–11.
- [38] Z.Q. Wang, Y.C. Gao, Large strain field near a notch-tip under tension, Theor. Appl. Fract. Mech. 26 (1997) 163–168, [https://doi.org/10.1016/S0167-8442\(96\)00045-6](https://doi.org/10.1016/S0167-8442(96)00045-6).
- [39] S. Graff, S. Forest, J.-L. Strudel, C. Prioul, P. Pilvin, J.-L. Béchade, Strain localization phenomena associated with static and dynamic strain ageing in notched specimens: experiments and finite element simulations, Mater. Sci. Eng. A 387–389 (2004) 181–185, <https://doi.org/10.1016/j.msea.2004.02.083>.
- [40] D. Moiseenko, P. Maksimov, S. Panin, V. Panin, Effect of notch shape on strain localization in steel under shock loading: hybrid CA simulation, AIP Conf. Proc. 1785 (2016), <https://doi.org/10.1063/1.4967097>, 040040–1–040040–4.
- [41] K.B. Broberg, On stable crack growth, J. Mech. Phys. Solids 23 (1975) 215–237, [https://doi.org/10.1016/0022-5096\(75\)90017-4](https://doi.org/10.1016/0022-5096(75)90017-4).
- [42] G.R. Johnson, W.H. Cook, A constitutive model and data for metals subjected to large strains, high strain rates and high temperatures, in: Proc. 7th Int. Symp. On Ballistics, Hague, Netherlands, April 1983, pp. 541–547.